International Journal of Thermodynamics (IJoT)*(8 pt Arial Bold)*
ISSN 1301-9724 / e-ISSN 2146-1511
www.ijoticat.com

Vol. 24 (No. 1), pp. 31-52, 2021
doi: 10.5541/ijot.776478
Published online: March 1, 2021

Thermal and Exergetic Study of the Integrated "Multi-Effect Desalination"- "Solar Rankine Cycle" System for the Iranian Southern Coastal Regions

S. Safa[1], K. Mobini[1], M. H. Khoshgoftar Manesh[*2,3]

[1] Department of Mechanical Engineering, Shahid Rajaee Teacher Training University, Tehran, Iran
[2] Department of Mechanical Engineering, Faculty of Technology & Engineering, University of Qom, Qom, Iran
[3] Center of Environmental Research, University of Qom, Qom, Iran
E-mail: [2,3] m.khoshgoftar@qom.ac.ir

Received 21 August 2020, Accepted 24 February 2021

Abstract

The application of the integrated solar-energy-based systems for water desalination and power production to some Iranian coastal regions has been investigated. For this purpose, the Integrated Multi Effect Desalination (MED) and Solar Rankine Cycle (SRC) are used. This work investigates the effects of the main thermodynamic parameters on the systems located at the southern Iranian cities of Chabahar, Qeshm, Kish and Asaluyeh. For each selected sites, the net power output of the system is 50 MWe. The results show that total exergy destruction is the highest for steam generator and cavity receiver which is in the range of 61% to 64% in several cases. Also, the Chabahar has the less total exergy destruction and the freshwater production is about 270.8 kg/s as most production. In addition, at other sites, the integrated cycle can produce about 266.2 kg/s of freshwater. Furthermore, the most total exergy destruction is related to Asaluyeh.

Keywords: *Exergy; Integrated Systems; Solar Rankine Cycle; MED; Desalination.*

1. Introduction

Due to the fresh water crises in the dry regions governments try to solve water scarcity problems with solutions like water well drilling, cloud seeding [1]–[6], dam construction, water desalination and making pipelines for transporting water from other areas [7].

Iran is located in south-western Asia between the Caspian Sea in the north, and the Persian Gulf and the Gulf of Oman in the south. The country ranks as the second largest country in the Middle East (after Saudi Arabia) and has a population of about 80 million. The United Nations has currently classified Iran's water resources as vulnerable and its water stress in the moderately exploited degree. However, the water stress at the southern regions is in heavily exploited degree [8]. In this climatic condition, the possibility of occurring any kind of droughts is high. Any drought can cause intense damage to agriculture and to the industries like steel and Aluminium which are large sectors of the country's economy. Rainfall is the main water source of the country. The yearly rainfall is 413 billion cubic meters (bcm), but it is considerably different across the country, ranging from less than 50 mm at the central parts to about 1000 mm at the Caspian coastal region [9]. However, most of the country has a yearly precipitation of less than 100 mm. The next resource of freshwater in Iran is the underground water. In the recent years, excess usage of this resource due to rapid population growth and decrease of precipitation has put this resources in a critical situation [10].

It is obvious that the unlimited water resources are the oceans, but their main problem is they are out of standard range of salinity. Therefore, it would be most pleasant to solve the water scarcity issue by desalinating the seawater. The total capacity of the desalination plants in 1971 was only about 17.4 m^3/s. It significantly increased to 231.5 m^3/s in 1995 [11]. This indicates the rapid growth of desalination plants in the world. Distribution of the desalination plants shows that the countries with coastal regions are increasingly turning to the sea to supply their required freshwater [12]. Iran has long borderlines with three huge volumes of water. More than 10 million people live in the southern coastal regions where the temperature is high and the yearly rainfall is very low [13]. They suffer a water crises and the installation of desalination plants is a very promising scenario for these regions.

Most conventional desalination technologies are generally classified into two groups: thermal desalination and membrane-based desalination. Thermal desalination methods include multi-stage flashing (MSF) and multi effect distillation (MED)

*Corresponding Author

and the most common membrane-based desalination method is the reverse osmosis (RO).

Multi-stage flash distillation is based on heating seawater to boiling point. Then, by lowering pressure at each stage, part of the liquid flashes to vapour. The seawater inlet temperature of the first stage exceeds 100℃. The operation temperature of multi-effect distillation (MED) system is usually below 70℃ [7]. Evaporation occurs at each effect at low pressure and a temperature below the boiling point. Due to a higher operating temperature of MSF compared to MED, thermal efficiency of MED is higher [14].

In 1960, a MSF desalination plant was installed in Khark Island with the capacity of 1000 m^3/day. Then, several other plants were installed with total capacity of 50,000 m^3/day [15]. Table 1 shows the MED plants which were installed in the southern coastal areas of Iran from 2000 till 2014.

Table 1. Desalination plants in Iran [16]

location	Plant type	Capacity (m^3/s)	start of establish
Chabahar	MSF	0.35	2000
Bandar Abbas	MSF	0.03	2000
Asaluyeh	RO	0.116	2004
Chabahar-kenarak(phase1)	MSF	0.174	2006
Bandar Abbas(Persian gulf region)	RO	0.03	2006
Siri island	MED	0.014	2007
Bandar Abbas power plant II	MED	0.03	2005
Khuzestan(hendijan)	RO	0.06	2008
Lavan island	MED	0.03	2009
Kharak island	MED	0.004	2008
Asaluyeh(south pars phases 9&10)	MED	0.02	2008
Qeshm island	MED	0.023	2011
Zahedan	RO	0.231	2010
Faror island	RO	0.006	2013

There are significant concerns about the environmental effects of desalination plants. One of the important problems of desalination process is its high energy consumption. Oil and natural gas are two primary energy resources in Iran. Currently, a large amount of the country's water supply (especially in the southern coastal regions) is provided by the desalination plants which are driven by fossil fuels. Based on the International Energy Agency (IEA) report (2017), since 1970, the CO2 emission from fuel combustion in Iran has increased from 38.9 to 552.4 million tons in 2015 which shows an increase of 227% [17]. Therefore, attention must be paid to the high fuel consumption by the desalination plants and their greenhouse gas (GHG) emissions.

A solution to this problem is integration of desalination and power production systems working with renewable energy resources. According to several investigations, among all the renewable energies, solar energy has the highest potential in Iran[18], [19]. Iran is located on the belt of sun and receives a high amount of solar energy radiation. Its incoming solar radiation of only two months is equal to its total fossil fuels reservoirs. The average global solar irradiation in Iran is about 2000 kWh/m2 per year and has more than 2800 sunny hours per year [20]. As shown in Figure 1, the southern and eastern regions receive much more radiation than the northern regions and the central parts have the highest potential to extract solar energy [21]. Solar energy can be extracted as both thermal and electrical (photovoltaic) forms. Both solar photovoltaic (PV) and concentrating solar power (CSP) can be utilized for generating electricity in areas with high direct normal irradiation (DNI). CSP can provide the high temperature thermal energy required for electricity generation [22]. CSP system has the capacity for integration with other systems. The main advantage of CSP compared to other technologies is its ability to store energy in thermal energy storage (TES), which is used when the solar energy is not available, such as when it is cloudy and after sunset [23]. A suitable sensible heat storage material is the molten salt which has a high specific heat. There are several researches regarding heat storage integrated with solar systems [24], [25].

Therefore, the solar-powered cogeneration of fresh water and power seems to be the best option in Iran. Other than installation of new combined solar plants, there are other options like addition of desalination facilities to the existing power plants

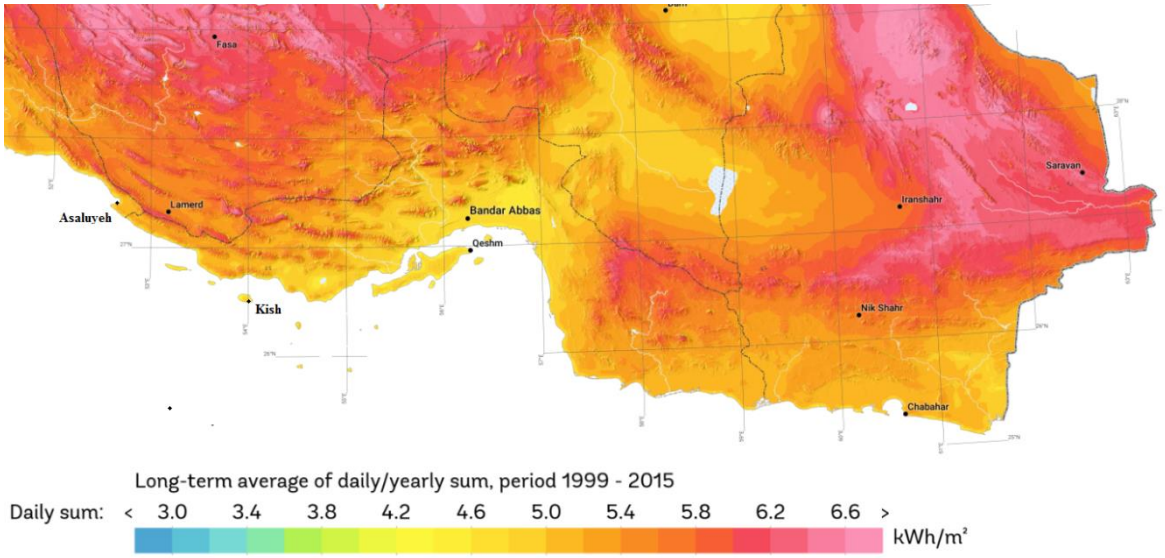

Figure 1. DNI solar resource map of Iran [21]

and addition of power plants to the existing desalination plants. In both the latter cases, it is possible to substitute solar energy with the existing fossil fuel consumption.

Many investigations have been done regarding the integration of CSP-desalination plants. The advantages of combining CSPs with desalination was studied by Trieb et al. for Mediterranean region [26] and integration of parabolic through collectors (PTC) in MENA region in [27]. They found that hybridization produces much less gas emissions than equivalent fossil fuel systems and supply sustainable and large-scale freshwater in these regions. Other investigations focused on the potential of desalinated water production via CSP-desalination in different zones such as the Gaza (Hamdan et al.) [28] and Oman (Gastli et al.) [29]. The integration of desalination and combined solar power tower in Cyprus and Greece, has been investigated by Alexopoulos and Hoffschmidt [30]. Palenzuela et al. proposed different integration of desalination units with parabolic CSP in Abu Dhabi [31]. They showed that the combination of CSP-MED plant is better than CSP-RO. A hybrid system for combined power and desalinated water production has been proposed by Demir and Dincer [32]. In this study, the combination of a MSF plant, a solar tower-natural gas plant and a Rankine cycle have been investigated.

The main purpose of the present study is to investigate the integration of a MED desalination system with a solar tower power plant. The MED system uses the steam exiting the 50 MW steam turbine. Therefore, the heat which is usually wasted in the condenser is used for desalination. This work investigates the effects of the main system parameters on the system performance using thermodynamic analysis. Four different southern coastal cities were selected for this study: Chabahar, Qeshm, Kish, and Asaluyeh.

2. Methodology

As shown in Figure 2, the system includes a heliostat field, a solar tower with a cavity receiver, a sensible thermal storage energy system, a solar-driven Rankine cycle and a MED unit. The heat transfer fluid (HTF) is a molten salt with composition of 59.5% LiCl and 40.5% KCl. The heliostat field reflects the Sun's normal direct beams and concentrates them to the top of the tower. The temperature on the receiver outlet surface reaches 667℃. The high temperature energy is absorbed by the receiver and transfers to the molten salt (HTF) which streams into a heat exchanger which works as a steam generator to supply the Rankine cycle. In the steam generator, water as working fluid enters with temperature 79℃ and absorbs the heat transferred from the HTF and turns into hot steam with a temperature of about 527℃ to drive the steam turbine and produce electricity. After passing through the steam generator, the molten salt temperature drops to 379℃. Then it is pumped to the receiver to begin a new cycle.

During the day and when the sky is clear, the molten salt coming from the tower passes through the full hot storage tank and then goes to the heat exchanger, after which it goes back to the solar tower. When DNI level is not sufficient, such as at the night or at cloudy weather, the molten salt flows to cold storage tank after the steam generator rather than going to the tower. It continues until the Sun shines again, when the cold storage content starts flowing to the receiver and the hot molten salt fills the hot storage tank. In the power cycle instead of a condenser, a MED unit have been used. This MED unit recovers the waste heat from steam and produces fresh water from seawater.

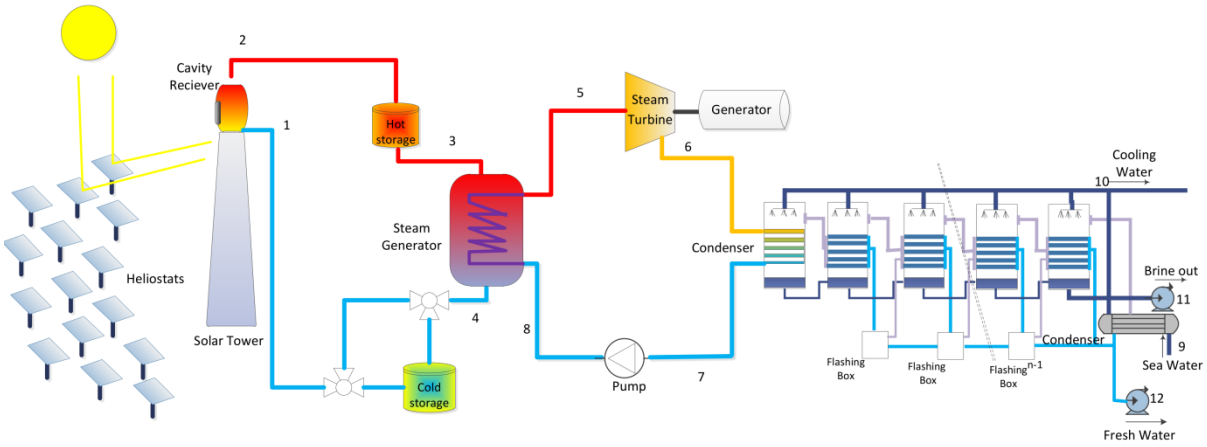

Figure 2. schematic diagram of the proposed integrated SRC-MED configuration

To calculate thermodynamic parameters, such as temperature, pressure, specific enthalpy, entropy, energy and exergy efficiencies and exergy destructions in the proposed energy system, Engineering Equation Solver (EES) Software has been used. The flowchart is shown in Figure 3.

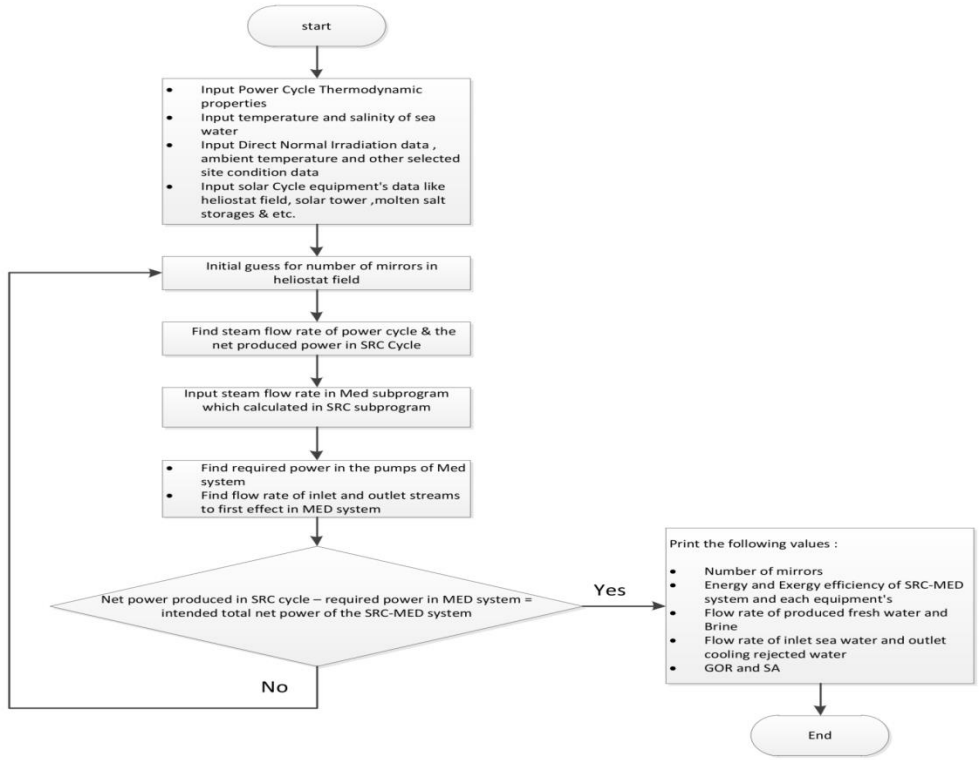

Figure 3. Flowchart for calculation of SRC-MED parameters

2.1 Direct normal irradiation

Table 2 contains the important data necessary for our calculations, including yearly averaged ambient temperature and DNI. The data are for the four chosen cities in the southern coastal regions of Iran and are directly obtained from solar GIS [21]. It is assumed that the yearly average daylight per day is 9 hours.

2.2 Heliostat field and solar power cycle

Nowadays, many types of solar tower such as volumetric, tubular and cavity receivers have been designed and studied by simulation and experimental methods. Among them, the cavity receivers working with molten salt has been recognized as the most cost-effective and efficient [33], [34].

It is assumed that a cavity receiver is located on the top of a tower with 140m height which is surrounded by a heliostat field. In the heliostat field depending on the position of heliostat to the tower, each heliostat has its own efficiency. The efficiency of entire heliostat field can be defined by using Eq. (1). The mechanisms for energy loss in the heliostat field include: the cosine effect, blocking, shading, atmospheric attenuation, mirror absorption/aberration and spillage [35]. In this study, a constant field efficiency of 75% has been assumed [36]. The total incident energy on the cavity receiver is obtained by Eq. (3).

$$\eta_{field} = \eta_{cos} \cdot \eta_{shadow} \cdot \eta_{block} \cdot \eta_{ref} \cdot \eta_{att} \cdot \eta_{spill} \quad (1)$$

$$\eta_{field} = \frac{Q_{rec,in}}{Q_{field}} \quad (2)$$

$$Q_{field} = DNI \times A_{field} \quad (3)$$

Table 2. Properties of the coastal sites located in the south of Iran

Region	latitude	Longitude	Altitude (m)	Ambient Temp.(C) [40]	Seawater Temp. (C) [37][38][39]	Seawater Salinity (ppm)	DNI (kWh/m^{2}day) [21]	Average daylight (hour)
Chabahar	25.29469	60.64406	32	29	30	36000[42]	4.803	8:42'[41]
Qeshm	26.78168	55.95004	95	32	35	41000[43]	4.904	8:25'[41]
Kish	26.54032	53.96037	27	30	35	41000[43]	4.704	8:45'[44]
Asaluyeh	27.52286	52.58819	30	25	35	41000[43]	5.21	8:45'[41]

The energy balance for the molten salt cavity receiver is presented in Eq. (4) [36]. As the HTF absorbs energy, energy lost by heat transfer mechanisms shown in Eq. (5).

$$Q_{rec.in} = Q_{loss.tot} + Q_{abs} \quad (4)$$

$$Q_{loss.tot} = Q_{loss.cond} + Q_{loss.conv} + Q_{loss.rad} + Q_{loss.reflect} \quad (5)$$

$$\eta_{rec} = \frac{Q_{abs}}{Q_{rec,in}} \quad (6)$$

$$Q_{rec.in} = A_{rec.surf}\left(\frac{T_{rec,surf} - T_{ms}}{\frac{d_o}{d_i h_{ms}} + \frac{d_o}{2\lambda_{rec,tube}} ln\frac{d_o}{d_i}}\right) \quad (7)$$

$$T_{ms} = \frac{T_{rec.in} + T_{rec.out}}{2} \quad (8)$$

$$Nu_{ms} = 0.023 Re_{ms}^{0.8} Pr_{ms}^{0.4} = \frac{h_{ms} d_i}{k_{ms}} \quad (9)$$

According to Li et al. [45], cavity receiver efficiency varies between 70% and 90%. Here, it is assumed that the receiver efficiency is about 80%.

The molten salt mass flow rate obtained from Eq. (10) has been used in Eq. (11) to determine the steam flow rate.

$$Q_{abs} = Q_{molten\ salt} = \dot{m}_{ms} \times C_{p_{ms}} \times (T_2 - T_1) \quad (10)$$

In the steam generator : $Q_{molten\ salt} = Q_{steam} = \dot{m}_{st}(h_5 - h_8) = \dot{m}_{ms}(h_3 - h_4)$ (11)

The design parameters of the solar power system are given in Table 3.

The following assumptions are used for thermodynamic calculations:

• The system is working in steady state with constant solar insulation and no chemical reaction occurs in the system.

• The changes in kinetic and potential energies and exergies are neglected.

• The heat losses occur only in molten salt tanks and the solar receiver.

• The pressure drop within the heat transfer fluid thermal cycle is neglected[46]

Due to heat loss in the storage tanks, a two-degree drop in HTF temperature has been assumed for both hot and cold tanks.

Solar multiple (SM) is a parameter that is used to oversize the solar field to provide the power demanded by the Rankine cycle. This parameter is defined as ratio of the thermal energy sent by the solar field at the design point, $P_{th,field}$ and the heat required by the Rankine cycle to work under nominal conditions, P_{th} (see Figure 4):

$$SM = \frac{P_{th,field}}{P_{th}} \quad (12)$$

In this work, it has been assumed that SM=1.8 [47].

Table 3. Design point parameters of the solar system

parameter	Unit	Value
Atmospheric pressure	atm	1
Area of the heliostat mirror	m^2	10*10
Heliostat field efficiency	%	75%
Tower height	m	140
Surface area of the solar receiver	m^2	50
Specific heat of the molten salt (at 500°C)	Kj/KgK	1.202
Receiver inlet temperature	K	650
Receiver outlet temperature	K	940
Receiver tube outside diameter	m	0.04
Receiver tube thickness	m	0.00125
Receiver tube thermal conductivity	W/mK	0.29
Receiver thermal power*	MW	272
Solar multiple		1.8
Steam generator inlet temperature	K	600
Steam generator outlet temperature	K	352

This number should obtain in respect of the solar multiple and rankine cycle efficiency ((50/.33) 1.8 = 272 MW).

To evaluate performance of the solar system components, exergy losses and destruction for these elements are defined in Table 4.

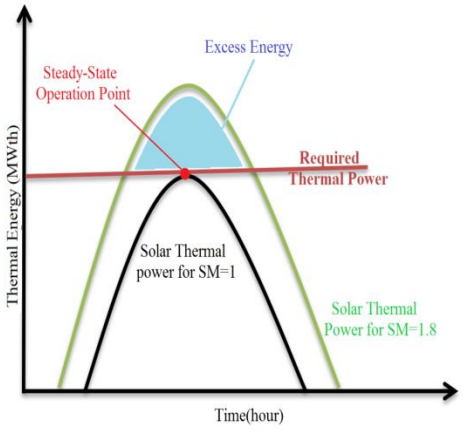

Figure 4. Thermal power energy delivered by the solar field at different solar multiple values [47]

2.3 Rankine cycle

The Rankine cycle is a determining element in the solar tower power plant and the other components of the solar system have to match with it. The other components simply try to serve the demands of the Rankine cycle. The main design parameters applied to the simulation of the steam Rankine power cycle are determined in Table 5.

The Rankine cycle components have been studied by assuming steady-state and steady-flow (SSSF)conditions.

Table 4.Exergy definitions of the solar system components

Component	Exergy losses and destructions	Exergy efficiency
Cavity receiver	$\dot{m}_1 ex_1 + Q_{cavity,rec}\left(1 - \frac{T_0}{T_{rec,surf}}\right) = \dot{m}_2 ex_2 + I_{dis.}$	$\eta_{II} = \frac{\dot{m}_2 ex_2 - \dot{m}_1 ex_1}{Q_{cavity,rec}\left(1 - \frac{T_0}{T_{rec,surf}}\right)}$
Hot molten salt	$\dot{m}_2 ex_2 = \dot{m}_3 ex_3 + I_{dis.}$	$\eta_{II} = \frac{\dot{m}_3 ex_3}{\dot{m}_2 ex_2}$
Cold molten salt	$\dot{m}_4 ex_4 = \dot{m}_1 ex_1 + I_{dis.}$	$\eta_{II} = \frac{\dot{m}_1 ex_1}{\dot{m}_4 ex_4}$
Steam generator	$\dot{m}_3 ex_3 - \dot{m}_4 ex_4 = \dot{m}_5 ex_5 - \dot{m}_8 ex_8 + I_{dis.}$	$\eta_{II} = \frac{\dot{m}_5 ex_5 - \dot{m}_8 ex_8}{\dot{m}_3 ex_3 - \dot{m}_4 ex_4}$

And with neglecting kinetic and potential energy, the energy balance for each component is:

$$\dot{Q} + \sum \dot{m}_i (h + \frac{v^2}{2} + gz)_i = \dot{W} + \sum \dot{m}_o (h + \frac{v^2}{2} + gz)_o \quad (13)$$

$$\left(\sum_{in} \dot{Q} - \sum_{out} \dot{Q}\right) - \dot{W} = \left(\sum_{in} \dot{m}h - \sum_{out} \dot{m}h\right) \quad (14)$$

$$\sum \dot{m}_i = \sum \dot{m}_o \quad (15)$$

The turbine power ($\dot{W}_{tur}$) and outlet enthalpy of the steam turbine ($h_{tur,out}$) based on isentropic efficiency ($\eta_{tur,isen}$) are respectively calculated as follows:

$$\dot{m}_{steam}\,(h_{tur.in} - h_{tur.out}) = \dot{W}_{tur} \quad (16)$$

$$\eta_{tur,ise} = \frac{h_{tur.in} - h_{tur.out-actual}}{h_{tur.in} - h_{tur.out-isen}} \quad (17)$$

Where $\eta_{tur,ise}$ is the isentropic efficiency of the turbine.

Table 5.Main design point parameters for the Steam Rankine cycle

parameter	Unit	Value
Net power production (W_{net})	MW	50
Turbine inlet temperature (T_5)	K	600
Turbine inlet pressure (P_5)	kPa	10000
Isentropic efficiency of turbines/ pumps	%	0.8
Rankine cycle efficiency	%	0.33

The work required by the pump in the power cycle to compress the working fluid was calculated via:

$$\dot{W}_{pump} = \dot{m}_{steam}\left(h_{pump.in} - h_{pump.out}\right) = \frac{v(P_{in} - P_{out})}{\eta_{isen.pump}} \quad (18)$$

$$\eta_{pump,ise} = \frac{h_{pump.out-isen} - h_{pump.in}}{h_{pump.out-actual} - h_{pump.in}} \quad (19)$$

Where $\eta_{pump,isen}$ the isentropic efficiency of pump.

The exergy destruction and loss rates and exergy efficiencies of the steam Rankine cycle components are defined in Table 6.

Table 6. Exergy definitions of the Rankine cycle components[48]

Component	Exergy losses and destructions	Exergy efficiency
Turbine	$\dot{m}_5 ex_5 = \dot{m}_6 ex_6 + \dot{W}_{tur} + I_{dis.}$	$\eta_{II} = \frac{\dot{W}_{tur}}{\dot{m}_5 ex_5 - \dot{m}_6 ex_6}$
pump	$\dot{m}_7 ex_7 + \dot{W}_{pump} = \dot{m}_8 ex_8 + I_{dis.}$	$\eta_{II} = \frac{\dot{m}_8 ex_8 - \dot{m}_7 ex_7}{\dot{W}_{pump}}$
Brine heater	$\dot{m}_f ex_{f,e1} + \dot{m}_6 ex_6 - \dot{m}_7 ex_7 = \dot{m}_{d,e1} ex_{d,e1} + \dot{m}_{b,e1} ex_{b,e1} + I_{dis.}$	$\eta_{II} = \frac{\left(\dot{m}_{d,e1} ex_{d,e1} + \dot{m}_{b,e1} ex_{b,e1}\right) - \dot{m}_f ex_{f,e1}}{\dot{m}_6 ex_6 - \dot{m}_7 ex_7}$

2.4 Multi effect desalination system

In this study, a multi-effect parallel/cross-feed distillation (MED) plant has been used as the desalination system and attached to the power solar cycle to produce fresh water. One of the most important advantages of this type of desalination system is the lower top brine temperature in the first effect which makes a lower condensing temperature for the Rankine cycle, allowing a better energy conversion and more electricity production in the power cycle. The number of effects is a parameter of the solution. A larger number of effects will need steam with more temperature and less electricity production and other hands produce more distillate water. In this system, effects and other components are coupled by mass and energy balances. Seawater enters into the effects in a parallel way at the same time after preheating in the condenser. In the first effect, seawater is sprayed and heated to boiling point by exhaust steam from the Rankine cycle which flows in the tubes, while some seawater also evaporates and supply the following effects' energy to the evaporating sea water. Brine and distillate vapor of each effect is passed on to the next effect. In the effects, the boiling point of water is lower than the top brine temperature by the boiling point elevation (BPE) which is a function of pressure and salinity. In the process, the steam condenses and condensates water in effects is collected and preheats entering sea water. Some seawater only has a cooling role in the condenser and exits the MED system after cooling collects the distilled water.

The MED mathematical model included mass balances, energy balances, and heat transfer equations for each effect and is developed considering the following assumptions:

The process is operating in a steady-state and steady-flow (SSSF) condition.

The temperature difference between all effects is assumed constant.

The specific heat of the water (C_p=4.18 KJ/kgK) and the latent heat of the vaporization of the water (λ_i) are assumed constant in all effects.

The effect of non-condensable gasses on heat transfer is neglected.

The non-equilibrium allowance (NEA) is negligible.

The distillate is salt-free.

There is no heat loss from any equipment to the environment.

Seawater temperature is considered the same as the cooling water temperature and dead-state temperature.

For simulations performed in this work, the desalination plants were considered besides the sea with a pipeline of under 1.5 km.

The maximum annual temperature was considered as the seawater temperature. Considering the assumptions stated previously, the mass, salinity, and energy balance can be written as follows:

$$T_1 = T_s - \Delta T_{pinch} \quad (20)$$

$$\Delta T = \frac{T_1 - T_n}{n-1} \quad (21)$$

$$T_i = T_{i-1} - \Delta T \quad (22)$$

$$f_i = \frac{F}{N} \;.\, i = 1. \ldots . n \quad (23)$$

For first effect,

$$B_1 = f_1 - D_1 \;,\; B_1 x_{B1} = x_{sw} f_1 \quad (24)$$

$$\dot{Q}_{motiv,steam} = D_1 \lambda_1 + f_1 (h_1 - h_f) \quad (25)$$

$$D_{i-1}\lambda_{i-1} + B_{i-1}\left(h_{B_{i-1}} - h_{B_i}\right) = D_i \lambda_i + f_i \left(h_i - h_f\right) \;.\, i = 2. \ldots . n \quad (26)$$

$$e^{ch} = \left(\sum mf_k \overline{e_k^{ch}}\right) + \bar{R}T_0 mf_k lnmf_k \quad (39)$$

$$x_{sw}\mathrm{f}_{i+1} + \mathrm{B}_i x_{Bi} = \mathrm{B}_{i+1}x_{Bi+1} \quad .i = 1. \ldots . n-2 \quad (27)$$

$$\mathrm{B}_{i+1} = \mathrm{f}_{i+1} - \mathrm{D}_{i+1} + \mathrm{B}_i - \mathrm{m}_{flash.i+1} \quad .i = 1. \ldots . n-1 \quad (28)$$

$$m_{flash.i} = \frac{(h_{Bi-1} - h_{Bi})}{\lambda_i}\ \mathrm{B}_{i-1} \quad .i = 2. \ldots . n-1 \quad (29)$$

$$d_{flash.i} = \frac{(h_{di-1} - h_{di})}{\lambda_i}\ \mathrm{D}_{i-1} \quad .i = 2. \ldots . n-1 \quad (30)$$

$$D_{tot} = \sum_{i-1}^{n} D_i + \sum_{i-1}^{n} m_{flash.i} - \sum_{i-1}^{n} d_{flash.i} \quad (31)$$

$$GOR = \frac{D_{tot}}{\dot{m}_s} \quad (32)$$

For condenser,

$$D_n\lambda_n = \dot{m}_{sw}\left(h_f - h_{sw}\right) \quad (33)$$

$$\dot{m}_{sw} = \dot{m}_{cw} + F \quad (34)$$

$$T_f = T_n - \Delta T_{mincon} \quad (35)$$

$$W_{pump,med} = (D_{tot} + B_n + f_{sw})(\frac{P_{amb} - P_n}{\rho\ \eta_{pump}}) \quad (36)$$

The specifications of the MED system are listed in Table 7.

Table 7. Design constraints for the distillation plant

parameter	Unit	Value
Motive steam temp. (T_s)	C	72
ΔT_{pinch}	C	3
ΔT_{mincon}	C	3
Density of sea water	Kg/m^3	998.2
Last effect temp.	C	46
Last effect salinity.	ppm	60000
Sea water temp.	C	---depends to --- site
Sea water salinity	ppm	42000
Isentropic efficiency of pumps	%	0.85
Distilled water temp.	C	40

In the MED system, exergy analysis according to exciting difference in salinity in effects, it should be considering the chemical exergy in

calculations. With neglecting kinetic and potential exergy we have:

$$e = e^{ph} + e^{ch} \quad (37)$$

The physical exergy of flow is computed by following definition:

$$e^{ph} = (h - h_0) - T_0(s - s_0) \quad (38)$$

Also, the chemical exergy of mixture is defined as follows:

Where mf_k is the molar ratio of the kth component and $\overline{e_k^{ch}}$ is the standard exergy of the kth component.

To compute the exergy of seawater, the specific entropy and enthalpy of a component per unit mole in an ideal solution at a specified temperature T and pressure P are defined as [49]:

$$s = mf_s\, s_s + mf_w\, s_w \quad (40)$$

$$h = mf_s\, h_s + mf_w\, h_w \quad (41)$$

Seawater can be assumed an ideal solution with sufficient accuracy. Thus, the entropy of a component per unit mole in an ideal solution at a specific pressure P and temperature T is:

$$s_i = s(P.T)_{pure} - R_u\ ln\, mf_i \quad (42)$$

Consequently, the chemical exergy of seawater is calculated by:

$$\mathrm{e}^{ch} = -N_m\, RT_0(mf_w\, lnmf_w + mf_s\, lnmf_s) \quad (43)$$

The exergy equations for the entire process with a summing $\dot{e}_{sea\ water} = 0$ can be derived as follows:

$$\dot{E}_{in} = \dot{m}_{steam,in}\,\dot{e}_{steam,in} + \dot{W}_{pump} \quad (44)$$

$$\dot{E}_{out} = \dot{m}_B\,\dot{e}_B + \dot{m}_{cw}\,\dot{e}_{cw} + \dot{m}_{Distilled}\,\dot{e}_{Distilled} + \dot{m}_{steam.out}\,\dot{e}_{steam.out} \quad (45)$$

$$\dot{E}_{fuel} = (\dot{m}_{steam.in}\,\dot{e}_{steam,in} - \dot{m}_{steam.out}\,\dot{e}_{steam.out}) + \dot{W}_{pump} \quad (46)$$

$$\dot{E}_{distroyed} = \dot{E}_{in} - \dot{E}_{out} \quad (47)$$

$$\dot{E}_{product} = \dot{m}_{Distilled}\,\dot{e}_{Distilled} \quad (48)$$

$$\epsilon = \frac{\dot{E}_{product}}{\dot{E}_{fuel}} * 100 \quad (49)$$

$$SA = \frac{A_{heat\ transfer\ area}}{freshwater\ flowrate}$$

Finally, the exergy efficiency of MED system can be presented as:

$$\eta_{II,MED} = \frac{\dot{m}_B\,\dot{e}_B + \dot{m}_{cw}\,\dot{e}_{cw} + \dot{m}_{Distilled}\,\dot{e}_{Distilled}}{\dot{E}_{fuel}} * 100 \quad (50)$$

3. Energy and exergy efficiencies

The total energy and exergy efficiencies of the integrated cycle can be obtained by input design point parameters. In the studied system, the only useful energy outputs of the system are net electricity produced by SRC and also fresh water. On the other hand, the only energy input to the cycle is the solar energy. Energy efficiency in this system can be obtained by Eq. (51):

$$\eta_{enrgetic} = \frac{\dot{W}_{net}}{\dot{Q}_{cycle}} = \frac{\dot{W}_{turbine} - \dot{W}_{pump}}{\dot{Q}_{solar}} \quad (51)$$

Where exergy efficiency takes into account external and internal irreversibility. The exergy efficiency in the system is required to optimize and improve cycle performance. The overal exergy efficiency of the cycle can be divided by equations 52 and 53[46][50]:

$$\eta_{II.exergetic} = 1 - \frac{\sum \dot{E}_{distroyed}}{\dot{E}_{\dot{Q}_{solar}}} \quad (52)$$

$$= \frac{E_{product}}{E_{fuel}} = \frac{W_{net.rankine} + E_{freshwater}}{\varphi_{rec.abs}}$$

$$\dot{E}_{\dot{Q}_{solar}} = Q_{rec.abs}\left(1 - \frac{T_0}{T_{rec.surface}}\right) \quad (53)$$

4. Results

To verify the thermodynamic simulation results by EES, the results of electricity production have been compared to the 20MWe Gemasolar solar power plant [51]. The properties of the Gemasolar and all other assumptions have been used from the validated model in the System Advisor Model (SAM) [52]and tabulated in Table 8. The results obtained from simulation show that the accuracy of EES codes is similar to that Gemasolar powerplant performances. The plant simulation results at the design point are presented in Figure 5, and the results of MED simulation as validated with Wang et al. [53]are demonstrated in Figure 6. It is evident that the results represent a good accordance with previous studies reported before with the maximum difference of 6% with the same conditions.

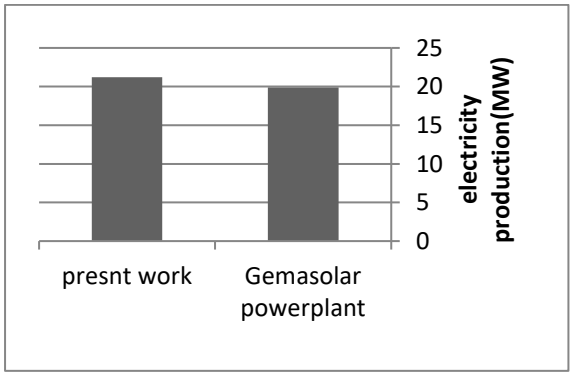

Figure 5. Comparison of the Solar driven Rankine cycle electricity production rate of the present work with Gemasolar power plant [51] for similar working conditions

Table 8. Design point characteristics of the 20MWe Gemasolar power plants [52]

parameter	Unit	Value
Heliostat field area	m^2	306658
Tower height	m	140
Receiver thermal power	MW_{th}	120
Receiver inlet temperture	C	290
Receiver outlet temperture	C	565
Solar multiple		2
Receiver surface	m^2	410
Turbine electrical power	MW_e	20
Turbine inlet pressure	kPa	10000
Receiver efficiency.	%	0.89
HTF		Sodium and potassium nitrates

In addition, the simulation of each case study has been compared with Thermoflex 23. The principal design point parameters used in the modeling and simulation of the solar system, Rankine cycle, and MED system are demonstrated in Tables 3, 5, and 7, respectively.

The important thermodynamic properties of the working fluids at state points in the cycles for selected sites are obtained and indicated in Tables 9-12, respectively.

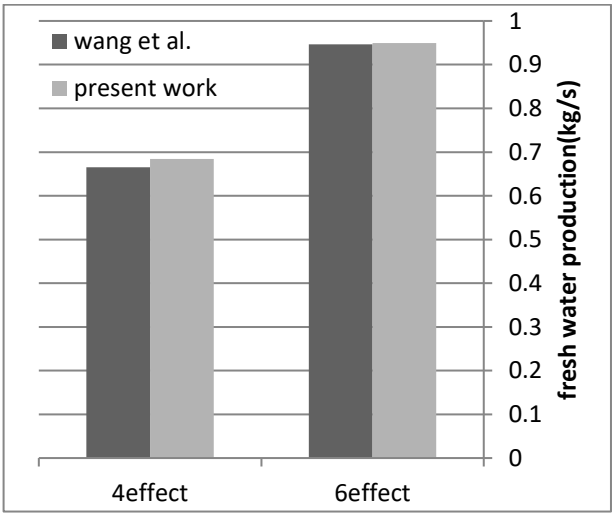

Figure 6. Comparison of the MED's fresh water production rate of the present work with that of Wang [53] for similar working conditions.

Table 9. Integrated cycle process data for Chabahar site

state	$\dot{m}\ (kg/s)$	$T(K)$	$P(kPa)$	$h(kJ/kg)$	s$(kJ/kg°K)$	Ė(KW)
1	492.3	650	100	26.51	0.0404	69073
2	492.3	940	100	375.1	0.4848	174644
3	492.3	938	100	372.7	0.4822	173846
4	492.3	652	100	28.91	0.0441	69711
5	54.1	800	10000	3443	6.684	77363
6	54.1	345	33.76	2504	7.364	15487
7	54.1	345	33.76	300.8	0.9775	629.8
8	54.1	352	10000	313.5	0.9849	1198
9	2064	303	100	119.6	0.4155	0
10	1395	316	100	171.5	0.5834	1487
11	396.5	319	100	163.4	0.5929	874
12	270.8	313	100	167.5	0.5723	833.8

Table 10. Integrated cycle process data for Qeshm site

state	$\dot{m}\ (kg/s)$	$T(K)$	$P(kPa)$	$h(kJ/kg)$	s$(kJ/kg°K)$	Ė(KW)
1	492.5	650	100	26.51	0.0404	67745
2	492.5	940	100	375.1	0.4848	172694
3	492.5	938	100	372.7	0.4822	171899
4	492.5	652	100	28.91	0.0441	68377
5	54.12	800	10000	3443	6.684	76375
6	54.12	345	33.76	2504	7.364	14368
7	54.12	345	33.76	300.8	0.9775	542.9
8	54.12	352	10000	313.5	0.9849	1110
9	3364	303	100	138.5	0.4761	0
10	2566	316	100	170.3	0.578	1027
11	530.3	319	100	163.4	0.5929	583.2
12	266.2	313	100	167.5	0.5723	684.6

Table 11. Integrated cycle process data for Kish site

state	$\dot{m}\ (kg/s)$	$T(K)$	$P(kPa)$	$h(kJ/kg)$	s$(kJ/kg°K)$	Ė(KW)
1	492.3	650	100	26.51	0.0404	68643
2	492.3	940	100	375.1	0.4848	174030
3	492.3	938	100	372.7	0.4822	173232
4	492.3	652	100	28.91	0.0441	69279
5	54.12	800	10000	3443	6.684	77049
6	54.12	345	33.76	2504	7.364	15117
7	54.12	345	33.76	300.8	0.9775	600.2
8	54.12	352	10000	313.5	0.9849	1168
9	3364	303	100	138.5	0.4761	0
10	2566	316	100	170.3	0.578	1027
11	530.3	319	100	163.4	0.5929	583.2
12	266.3	313	100	167.5	0.5723	684.6

Table 12. Integrated cycle process data for Asaluyeh site

state	$\dot{m}\ (kg/s)$	$T(K)$	$P(kPa)$	$h(kJ/kg)$	s$(kJ/kg°K)$	Ė(KW)
1	492.4	650	100	26.51	0.0404	70916
2	492.4	940	100	375.1	0.4848	177387
3	492.4	938	100	372.7	0.4822	176583
4	492.4	652	100	28.91	0.0441	71561
5	54.11	800	10000	3443	6.684	78742
6	54.11	345	33.76	2504	7.364	16999
7	54.11	345	33.76	300.8	0.9775	756.5
8	54.11	352	10000	313.5	0.9849	1327
9	3363	303	100	138.5	0.4761	0
10	2565	316	100	170.3	0.578	1027
11	530.2	319	100	163.4	0.5929	583.1
12	266.2	313	100	167.5	0.5723	684.5

The main outputs of proposed SRC cycel are freshwater, power, steam, molten salt flow rates' compression in selected sites with an equal heliostat field, the number of mirrors in heliostat field, energy and exergy efficiency, exergy lose and destruction, for integrated system and all its equipment under equal power production condition and MED system are the gain output ratio (GOR), specific surface areas of the effects (SA) and fresh water flow rate with constant inlet energy.

GOR the ratio of produced fresh water flow rate to the motive steam flow rate which entering into MED. As demonstrated in Figure 7, the maximum feasible fresh water can be a product with 6450 mirrors in the selected sites obtained in Asaluyeh about 23,842 m^3 per day and also the maximum feasible power production obtains in Asaluyeh by 34.6 MW. Figure 8 shows that it is maximum molten salt and steam flow rates exist to handle the cycle. Also, Figure 9 indicates that the number of mirrors in the heliostat filed under an equal 50MW power generation condition is the lowest in the case of Asaluyeh site by 8646. Based on the results, the Asaluyeh site has a suitable feasibility and promising scenario to establish the SCR power plant.

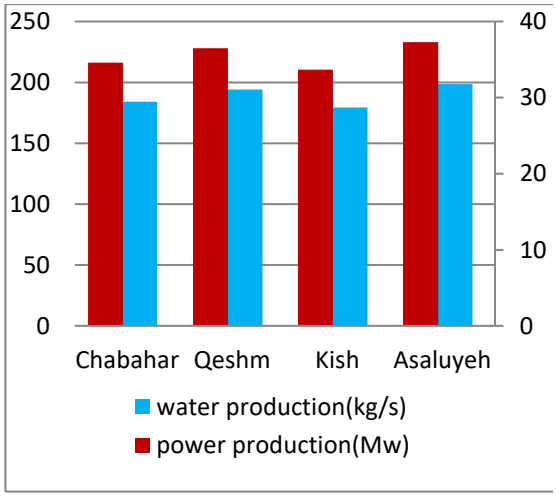

Figure 7. Comparison of water and power production in the selected sites with equal heliostat field

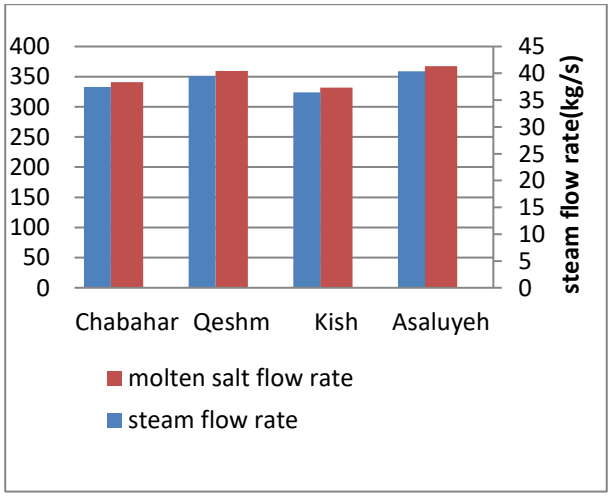

Figure 8.Comparison of steam and molten salt flow rates in the selected sites with equal heliostat field

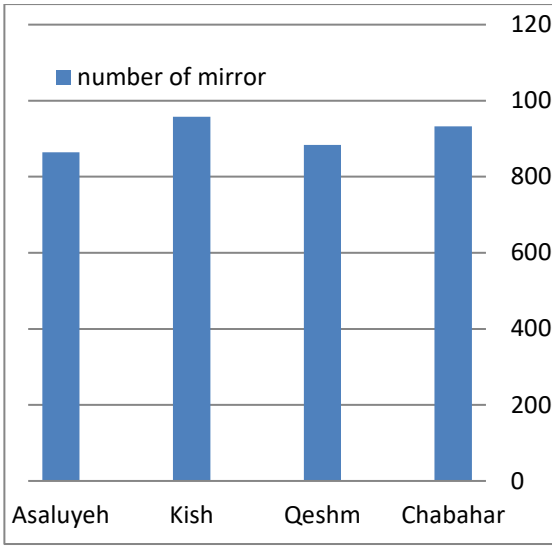

Figure 9. Required Number of mirrors for 50MW power generation

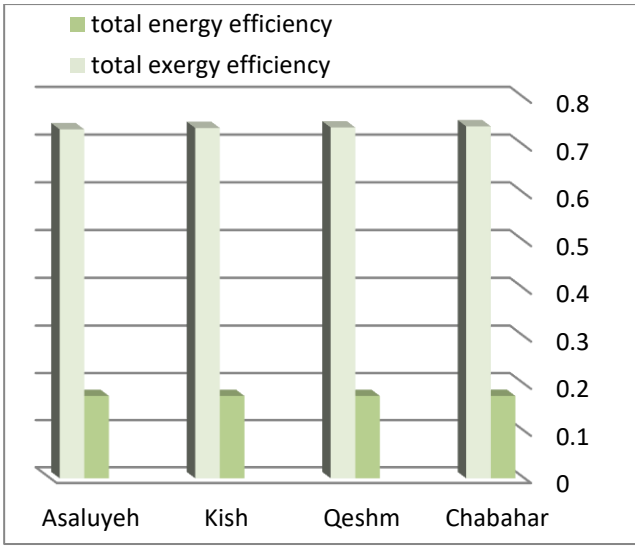

Figure 10.Comparison of total energy and Exergy efficiencies of the integrated cycles at the selected sites with 50MW power production and 6 MED effects

Total energy and exergy efficiencies for the whole integrated SRC-MED system are calculated for the selected sites. As indicated in Figure 10, the efficiencies in the selected sites are close and the best amounts with less than 1% difference are obtained for Chabahar which are about 17.5% and 74.06%, respectively, under an equal 50MW electricity production condition. Figure 11 shows that the total exergy loss and destruction rate of the system is maximum for Asaluyeh site and minimum for Chabahar site, equal to 72.078 MW and 70.313 MW, respectively. And also as Figure12 shows, the combined exergy efficiency in the selected sites are so close and the maximum rate obtained for Chabahar and minimum rate for other sites with less than 0.001% amount which are about 29.67% and 29.58%, respectively.

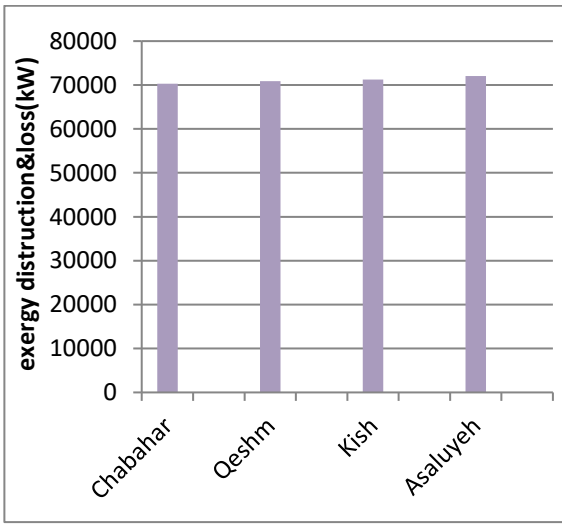

Figure 11. Total exergy destruction & losses for the selected sites under 50MW power production condition

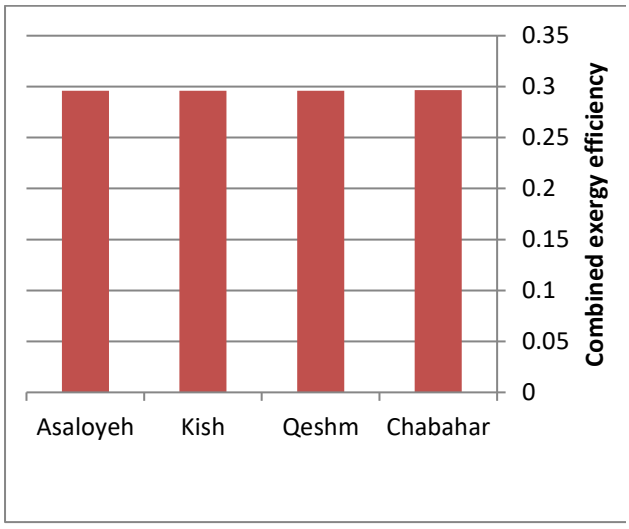

Figure 12. Total combined exergy efficiency for the selected sites under 50MW power production condition

Moreover, Figures 13 and 14 indicate the exergy efficiency and destruction for each element of the whole cycle. It is obvious that the storage tanks, with respect to their protective insulation that makes only a two-degree temperature difference between inlet and outlet streams, have the highest exergy

efficiency with an exergy destruction of about 635 kW to 800 kW in several cases where the steam generator, with respect to crossing high temperature flows, has the lowest exergy efficiency of about 73% from among the equipment with exergy destruction of about 27.606 MW to 28.258 MW in several cases.

According to the type of receiver, the exergy efficiency of the cavity receiver with respect to the highest temperature in the whole cycle is approximately 86%, ranking the second from among elements after storage tanks.

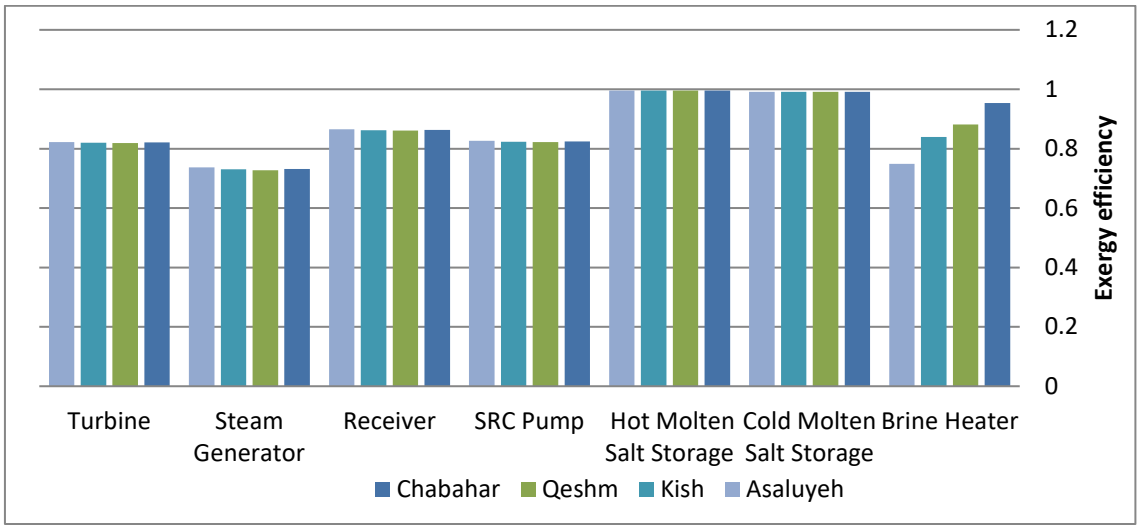

Figure 13. Comparison of exergy efficiency of the integrated cycles with 50MW power production and 6 MED effects at the selected sites

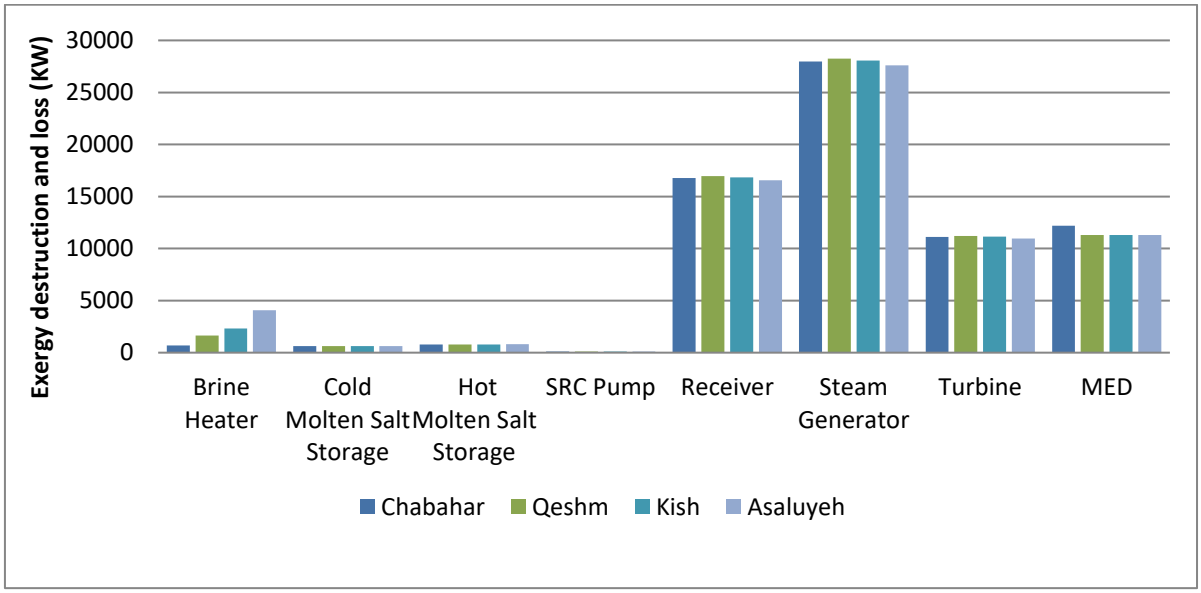

Figure 14. Exergy destruction & losses for the Integrated cycle components with 50MW power production and 6 MED effects at the selected sites

The fresh water producton per square meter of heliostat field for the selected sites calculated for the whole integrated SRC-MED system. As indicated in Figure 15, fresh water production per square meter of heliostat field in the selected sites are close and the best amounts with less than 0.26 Kg/m^{2}day difference are obtained for Asaluyeh with maximum DNI and minimum heliostat field among selected sites which are about 2.66 Kg fresh water/m^{2}day.

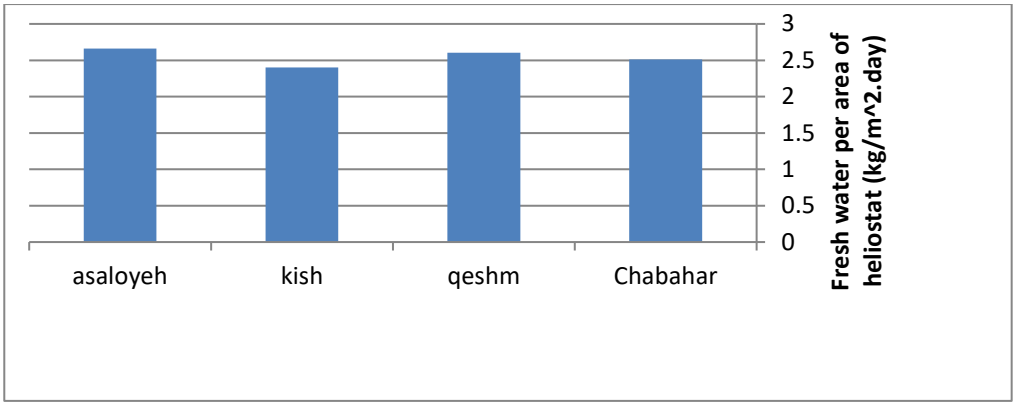

Figure 15. Fresh water per area of heliostat for the selected sites under 50MW power production condition

The exergy destruction and losses of each component for the selected sites are depicted in Figures 16-19. As demonstrated, the total exergy destruction and losses of the steam generator and cavity receiver comprise 61% to 64% in several cases. The receiver surface has the highest temperatures from among all cycle components. The highest exergy destruction and loss rates can be explained by the high heat transfer rates at higher temperatures and heat losses through the components. After them, the MED system and turbine have the highest exergy destruction with 17% and 15%, respectively. The exergy destruction and loss of the MED system caused by the great flow rate of the cooling rejected brine with the temperature of 40 °C are higher than the environmental temperature.

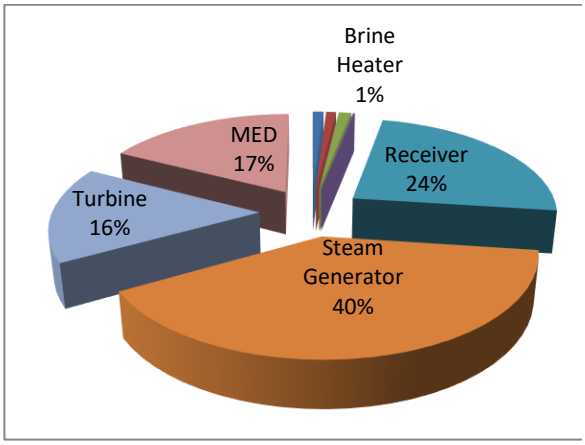

Figure 16. Percentages of exergy destruction & losses of the components of the Integrated cycle with 50MW power production and 6 MED effects at Chabahar site

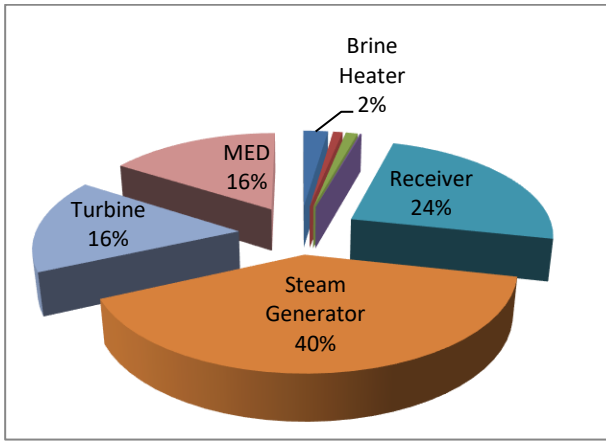

Figure 17. Percentages of exergy destruction & losses of the components of the integrated cycle with 50 MW power production and 6 MED effects at Qeshm site

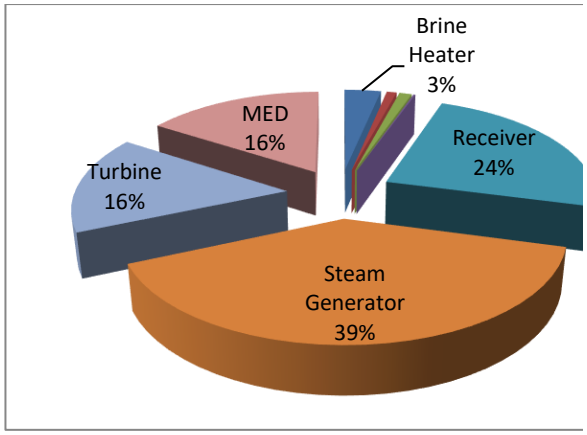

Figure 18. Percentages of exergy destruction & losses of the components of the Integrated cycle with 50MW power production and 6 MED effects at Kish site

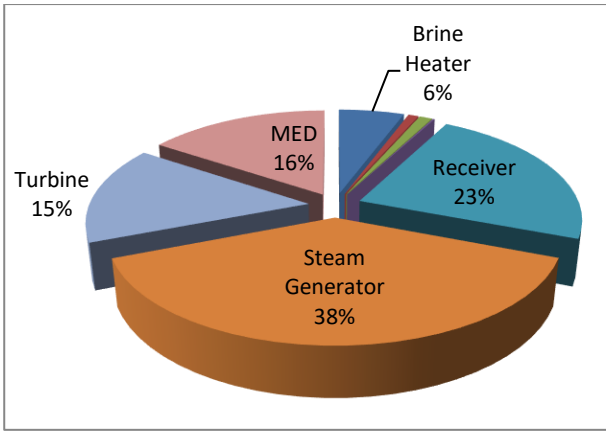

Figure 19. Percentages of exergy destruction & losses of the components of the Integrated cycle with 50MW power production and 6 MED effects at Asaluyeh site

For a fair comparison between the MED systems in the selected sites, the GOR and SA with considering 50 MW of power generation and six effects have been determined in Figures 20 and 21. It is evident that Chabahar MED system has maximum GOR and minimum SA from among others. Thus, it has minimum inlet energy and maximum fresh water production. Other integrated MED systems have the second place with small amounts of difference.

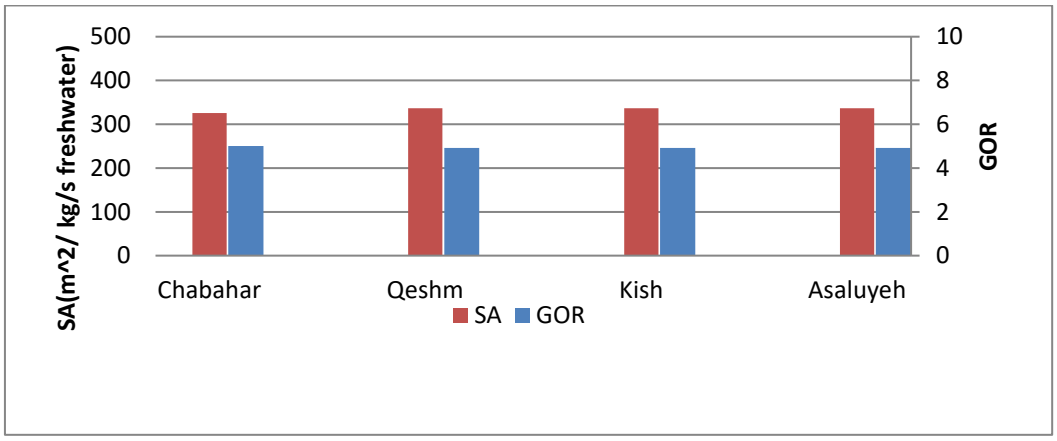

Figure 20. Comparison of GOR & SA of the MED systems used in the integrated cycles with 50MW power production and 6 MED effects at the selected sites

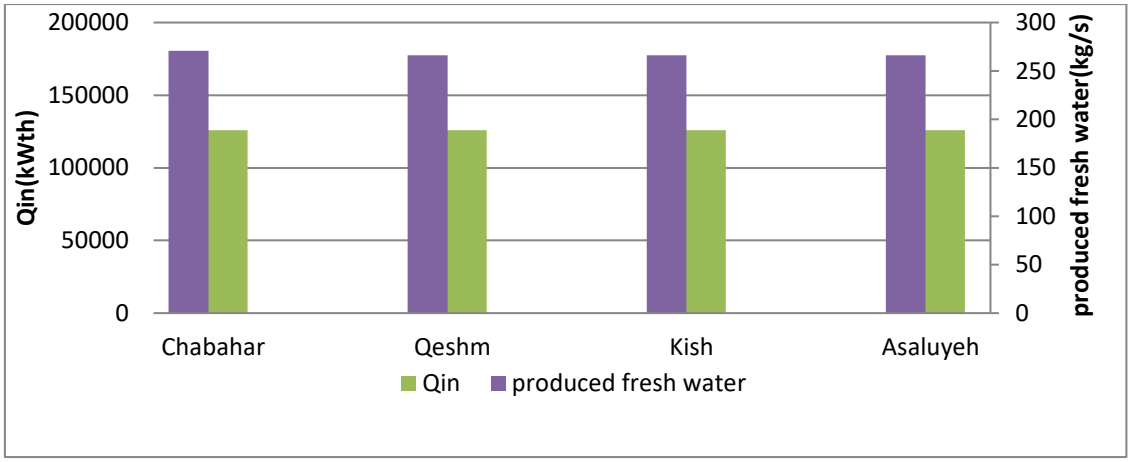

Figure 21. Comparison of Qin and produced fresh water in the MED systems of the integrated cycles with 50MW power production and 6 MED effects at the selected sites

The performance evaluation has been performed for the MED system based on GOR, SA, and fresh water in the selected site with a different effect. As indicated in Figures 22-25, with an increase in the number of effects, the GOR and SA increase.

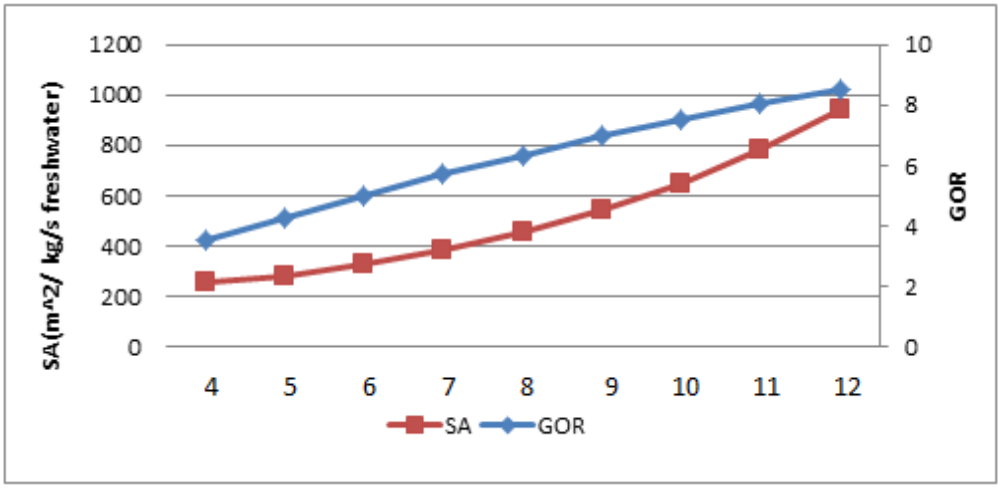

Figure 22. Med system outputs for diffrent effects in Chabahr site for constant Q_{in}

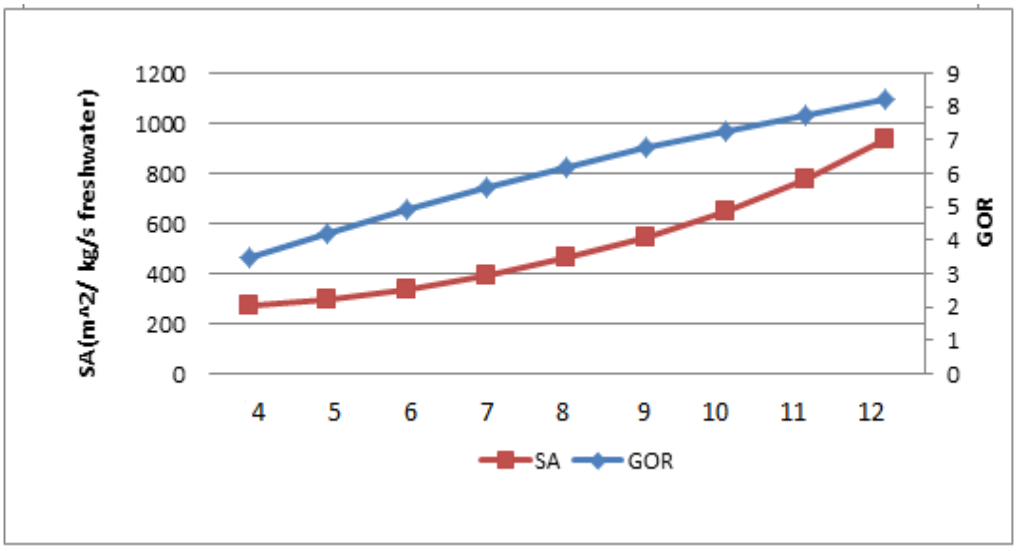

Figure 23. Med system outputs for diffrent effects in Qeshm site for constant Q_{in}

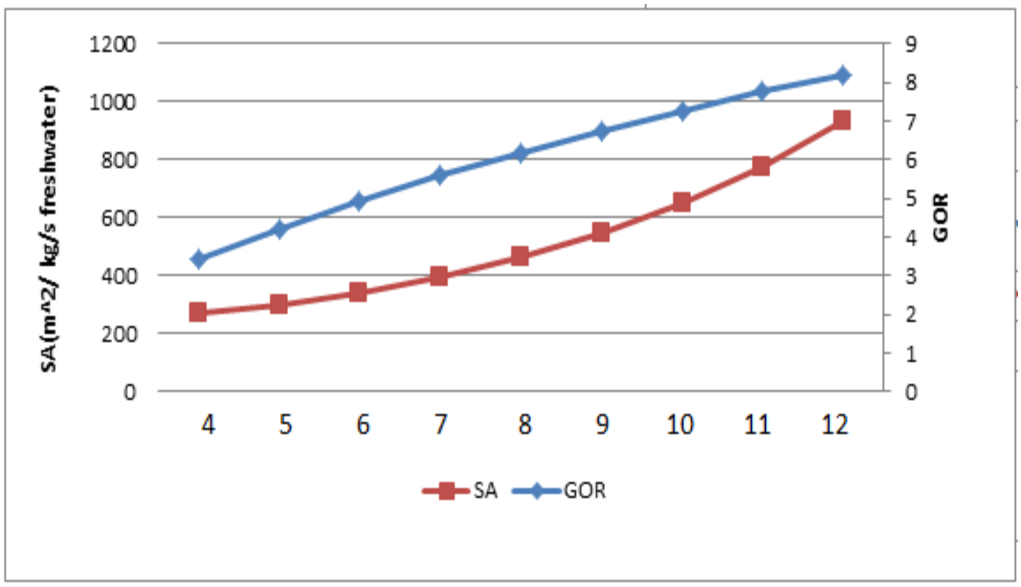

Figure 24. Med system outputs for diffrent effects in Kish site for constant Q_{in}

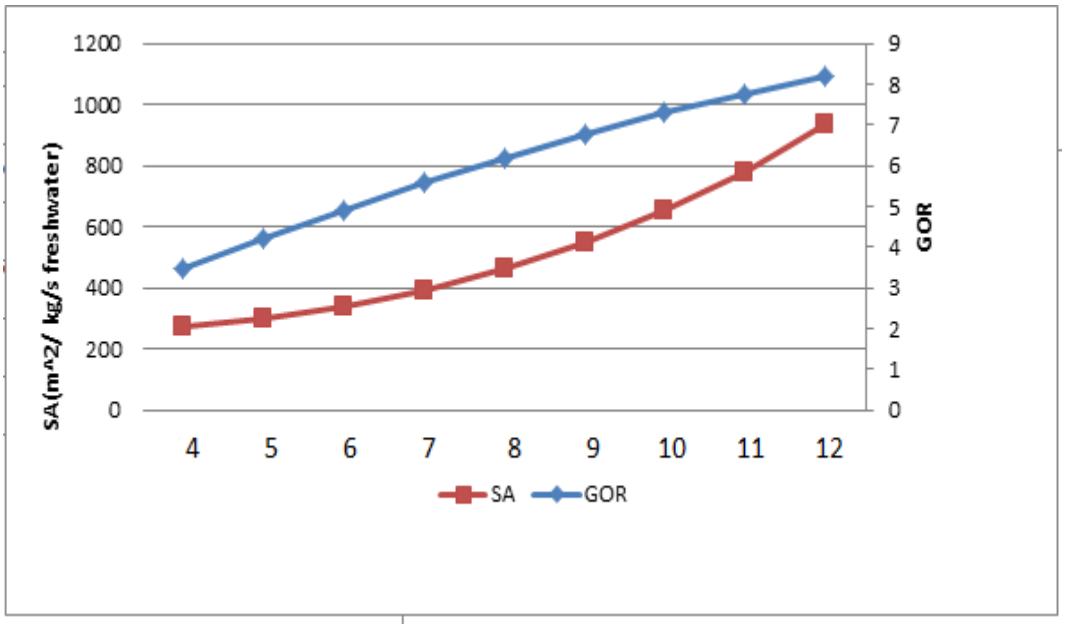

Figure 25.Med system outputs for diffrent effects in Asaluyeh site for constant Q_{in}

5. Conclusion

In this study, a combined potable water and power production system based on an integrated SRC-MED system is proposed for the Iranian Southern coastal region. Due to high thermal capacity and high heat transfer coefficient, LiCl/KCl molten salt mixture has been used in simulation. In this regard, thermodynamic simulation and exergy analysis have been performed in EES. The thermodynamic parameters, exergy destruction, and loss rates for each component of the system have been calculated for four cities. The results show that steam generator and cavity receiver contribute to most of the total exergy destruction and losses. To produce 50 MW of power, the number of mirrors in the heliostat filed is the smallest in the case of Asaluyeh site.

Fresh water production per square meter of heliostat field in the selected sites are close and the best amounts with less than 0.26 Kg/m^{2}day difference are obtained for Asaluyeh which are about 2.66 Kg fresh water/m^{2}day.

Chabahar has the less total exergy destruction and the most freshwater production is about 270.8 kg/s as most production. Furthermore, the most total exergy destruction is related to Asaluyeh.

In our future study, we intend to perform exergo-economic and exergo-environmental analyses. In addition, the optimization of the main thermodynamic parameters for the integrated system will be investigated.

6. Nomenclature

A	m^2	area
d	m	diameter of receiver tube
P	Mw	power
$\dot{W}$	Kj/s	work
E	W	exergy
h	J/kgK or W/m^2K	Enthalpy or convective heat transfer coefficient
C_p	kJ/kg °C	specific heat capacity
k	W/mK	thermal conductivity
$\dot{m}$	kg/s	mass flow rate
$\dot{m}_s$	kg/s	Motive steam mass flow rate
$\dot{m}_{ms}$	kg/s	Molten salt mass flow rate
Nu		Nusselt number
Re		Reynolds number
Pr		Prandtl number
Q	W	thermal energy
T	K	temperature
T_i	K	temperature of effect i
T_s	K	Motive steam temperature
T_f	°C	Feed water temperature
T_{cw}	°C	cooling water temperature
T_{sw}	°C	sea water temperature
ΔT	°C	temperature difference
$\Delta T_{mincond}$	°C	temperature difference in condenser
U	$kw/m^2°C$	heat transfer coefficient
U_{cond}	$kw/m^2°C$	heat transfer coefficient at condenser
U_i	$kw/m^2°C$	heat transfer coefficient in each effect
V	m/s	velocity
z	m	height
g	m/s^2	gravity
D_i	kg/s	distilled mass flow rate from effect i
F_i	kg/s	Feed mass flow rate from effect i
B_i	kg/s	Brine mass flow rate from effect i
x	Kg/kg	salinity
N		Number of effect's or moles
R	J/ K. mol	gas constant

Greek symbols

λ	W/mK or kJ/kg	Conductivity or latent heat
ρ	[kg /m^3]	density
η_{field}		heliostat field efficiency
η		energetic efficiency
η_{II}		exergetic efficiency
Δ		difference

Subscripts

abs	absorbed
amb	ambient
cond	Conduction or Condenser
conv	convection
rad	radiation
reflect	reflection
rec	receiver
field	heliostat field
tur	turbine
isen	isentropic
th	thermal
i	in
o	out
m	mole
in	inlet, inner
out	Outlet, outer
ms	molten salt
s	steam
rec,in	receiver inlet

rec,out	receiver outlet
rec, surf	receiver surface
cond	condenser
sw	Sea water
cw	Cooling water
f	Feed water
mincon	Minimum of condenser
ph	physical
ch	chemical
mf	Molar friction

Abbreviations

DNI	W/m^{2}day	direct normal irradiation
TES		thermal energy storage
SM		Solar multiple
LMTD		log mean temperature difference
SRC		solar Rankine cycle
GOR		Gain Output Ratio
SA		Specific surface area of the MED system

Appendix

Appendix A. Correlations for seawater thermodynamic properties calculation

Correlations of seawater thermodynamic properties such as specific entropy and specific enthalpy are given in this section.

A.1. Specific enthalpy

The enthalpy of seawater is calculated by the following equation which is valid for 0 ≤ x ≤ 0.12 kg/kg and 10 ≤ T ≤120 ℃ [54].

$$h_{sw} = h_w - 0.001x(b_1 + b_2x + b_3x^2 + b_4x^3 + b_5T + b_6T^2 \ldots + b_7T^3 + b_8T\ x + b_9T\ x^2 + b_{10}T^2\ x)$$

$$b_1 = -2.348 \times 10^4;\ b_2 = 3.152 \times 10^5;\ b_3 = 2.803 \times 10^6;$$

$$b_4 = -1.446 \times 10^7;\ b5 = 7.826 \times 10^3;\ b_6 = -4.417 \times 10^1;$$

$$b_7 = 2.139 \times 10^1;\ b_8 = -1.991 \times 10^4;\ b_9 = 2.778 \times 10^4;$$

$$b_{10} = 9.728 \times 10^1;$$

In this equation T is the temperature of the effect and x is the salinity of the brine in the same effect and h_w is the enthalpy of pure water.

A.2. Specific entropy

The entropy of seawater is given by following equation which is valid for 0 ≤ x ≤ 0.12 kg/kg and 10 ≤ T ≤120 ℃ [54].

$$s_{sw} = s_w - x(a_1 + a_2x + a_3x^2 + a_4x^3 + a_5T + a_6T^2 \ldots + a_7T^3 + a_8T\ x + a_9T\ x^2 + a_{10}T^2\ x)$$

$$a_1 = -4.231 \times 10^2;\ a_2 = 1.463 \times 10^4;\ a_3 = -9.88 \times 10^4;$$

$$a_4 = 3.095 \times 10^5; a_5 = 2.562 \times 10^1;\ a_6 = -1.443 \times 10^{-1};$$

$$a_7 = 5.879 \times 10^{-4};\ a_8 = -6.111 \times 10^1;\ a_9 = 8.041 \times 10^1;$$

$$a_{10} = 3.035 \times 10^{-1};$$

In this equation s_w is the entropy of pure water.

Appendix B. Boiling point elevation (BPE) in MED

The raise in the water boiling temperature at a given pressure due to dissolved salts in the water is called the boiling point elevation (BPE). The following formula is used to calculate BPE [55].

$$BPE = AX + BX^2 + CX^3$$

$$A = 0.0825 + (0.0001883 \times T) + (0.00000402 \times T^2)$$

$$B = -0.0007625 + (0.0000902 \times T) - (0.00000052 \times T^2)$$

$$C = 0.0001522 - (0.000003 \times T) - (0.00000003 \times T^2)$$

Where T and X depict temperature of the effect and salinity of the brine in the same effect, respectively.

Appendix C. Heat transfer area calculation

The heat transfer area for each effect in the MED system, A, can be obtained from the following equation [55]:

$$A = \frac{Q_{motive,steam}}{U\Delta T_{LM}}$$

In this equation, A, U, $Q_{motive,steam}$ and ΔT_{LM} represent heat transfer area, overall heat transfer coefficient, inlet motivating heat from the inlet steam and log-mean temperature difference, respectively. The logarithmic mean temperature difference can is calculated by:

$$\Delta T_{LM} = \frac{\Delta T_{max} - \Delta T_{min}}{\ln(\frac{\Delta T_{max}}{\Delta T_{min}})}$$

The overall heat transfer coefficients for each effect and for the condenser of MED system are

respectively given by the following correlations [55]:

$$U_i = 0.001 * (1969.5 + (12.057 * T_i) - (0.085989 * T_i^2) + (0.00025651 * T_i^3))$$

$$U_{cond} = 0.001 * \left(1719.4 + \left(3.2063 * T_{sat,n}\right) + \left(0.01597 * T_{sat,n}^2\right) - \left(0.00019918 * T_{sat,n}^3\right)\right)$$

T_i is the temperature of the effect and $T_{sat,n}$ is the vapor saturation temperature at the last effect. The logarithmic mean temperature difference (ΔT_{LM}) of the condenser is calculated by:

$$\Delta T_{LM_{cond}} = \frac{(T_n - T_f) - (T_n - T_{sw})}{\ln(\frac{T_n - T_f}{T_n - T_{sw}})}$$

Where the subscripts sw, f and n represent sea water, feed sea water and the last effect, respectively.

7. References

[1] T. P. DeFelice *et al.*, "Extra area effects of cloud seeding - An updated assessment," *Atmospheric Research*, vol. 135–136. Elsevier, pp. 193–203, 01-Jan-2014.

[2] M. Lompar, M. Ćurić, D. Romanic, L. Zou, and H. Liang, "Precipitation enhancement by cloud seeding using the shell structured TiO2/NaCl aerosol as revealed by new model for cloud seeding experiments," *Atmos. Res.*, vol. 212, pp. 202–212, Nov. 2018.

[3] T. P. DeFelice *et al.*, "Extra area effects of cloud seeding — An updated assessment," *Atmos. Res.*, vol. 135–136, pp. 193–203, Jan. 2014.

[4] J. R. Kulkarni, S. B. Morwal, and N. R. Deshpande, "Rainfall enhancement in Karnataka state cloud seeding program 'Varshadhare' 2017," *Atmos. Res.*, vol. 219, pp. 65–76, May 2019.

[5] C. Hutchinson and S. Herrmann, *The future of arid lands-revisited: a review of 50 years of drylands research*. 2007.

[6] C. Agnew and P. Woodhouse, *Water resources and development*. Routledge, 2011.

[7] S. A. Kalogirou, "Seawater desalination using renewable energy sources," *Prog. Energy Combust. Sci.*, vol. 31, no. 3, pp. 242–281, Jan. 2005.

[8] A. Pugsley, A. Zacharopoulos, J. D. Mondol, and M. Smyth, "Global applicability of solar desalination," *Renew. Energy*, vol. 88, pp. 200–219, 2016.

[9] S. Assadollahi, "Groundwater resources management in Iran," *... Spec. Sess. Groundw. 5Th ...*, pp. 1–16, 2009.

[10] K. Madani, "Iran's Water Crisis: Inducers, Challenges and Counter-Measures," in *ERSA 45th Congress of the European Regional Science Association*, 2005, pp. 1–20.

[11] A. Zirakrad, S. J. Hashemian, and M. T. Ghaneian, "Performance Study of Reverse Osmosis Plants for Water Desalination in Bandar-Lengeh, Iran," *J. Community Heal. Res.*, vol. 2, no. 1, pp. 8–14, 2013.

[12] A. D. Khawaji, I. K. Kutubkhanah, and J. M. Wie, "Advances in seawater desalination technologies," *Desalination*, vol. 221, no. 1–3, pp. 47–69, Mar. 2008.

[13] A. Pak and M. Farajzadeh, "Iran's Integrated Coastal Management plan: Persian Gulf, Oman Sea, and southern Caspian Sea coastlines," *Ocean Coast. Manag.*, vol. 50, no. 9, pp. 754–773, Jan. 2007.

[14] M. A. Darwish and A. Alsairafi, "Technical comparison between TVC/MEB and MSF," *Desalination*, vol. 170, no. 3, pp. 223–239, Nov. 2004.

[15] M. Emami, G. H. Jalali Ghajar, and N. Kaynia, "State of desalination projects in Iran," *Desalination*, vol. 23, no. 1–3, pp. 465–470, Jan. 1977.

[16] Reports, "WATER INDUSTRY SEGMENT REPORT DESALINATION," *World Trade Cent. San Diego*, no. April, 2011.

[17] IEA Statistic, "CO2 emissions from fuel combustion–highlights," 2011.

[18] Mohsen Bahrami and Payam Abbaszadeh, "An overview of renewable energies in Iran," *Renew. Sustain. Energy Rev.*, 2013.

[19] M. Dehghani and M. Feylizadeh, "An overview of solar energy potential in Iran," *Int. J. Curr. Life Sci.*, vol. 4, no. 9, pp. 7173–7180, 2014.

[20] M. Bahrami and P. Abbaszadeh, "An overview of renewable energies in Iran," *Renewable and Sustainable Energy Reviews*, vol. 24. Pergamon, pp. 198–208, 01-Aug-2013.

[21] "Solar resource maps and GIS data for iran islamic Rep. | Solargis." [Online]. Available: https://solargis.com/maps-and-gis-data/download/iran. [Accessed: 08-Jun-2018].

[22] S. S. M. Tehrani and R. A. Taylor, "Off-design simulation and performance of

molten salt cavity receivers in solar tower plants under realistic operational modes and control strategies," *Appl. Energy*, vol. 179, pp. 698–715, Oct. 2016.

[23] J. Demailly and B. Nisman, "Attachement de l'ARN aux fragments de membrane d'Escherichia coli et fonction du complexe form??. I.," *Comptes rendus Hebd. des seances l"Academie des Sci. Ser. D Sci. Nat.*, vol. 268, no. 14, pp. 1878–1881, Sep. 1969.

[24] D. Laing, C. Bahl, T. Bauer, D. Lehmann, and W.-D. Steinmann, "Thermal energy storage for direct steam," in *Solar Paces 2009*, 2009.

[25] J. H. Peterseim, S. White, A. Tadros, and U. Hellwig, "Concentrated solar power hybrid plants, which technologies are best suited for hybridisation?," *Renewable Energy*, vol. 57. Pergamon, pp. 520–532, 01-Sep-2013.

[26] F. Trieb *et al.*, "Combined solar power and desalination plants for the Mediterranean region - Sustainable energy supply using large-scale solar thermal power plants," *Desalination*, vol. 153, no. 1–3, pp. 39–46, Feb. 2003.

[27] F. Trieb and H. Müller-Steinhagen, "Concentrating solar power for seawater desalination in the Middle East and North Africa," *Desalination*, vol. 220, no. 1–3, pp. 165–183, Mar. 2008.

[28] L. K. Hamdan, M. Zarei, R. R. Chianelli, and E. Gardner, "Sustainable water and energy in Gaza Strip," *Renewable Energy*, vol. 33, no. 6. Pergamon, pp. 1137–1146, 01-Jun-2008.

[29] A. Gastli, Y. Charabi, and S. Zekri, "GIS-based assessment of combined CSP electric power and seawater desalination plant for Duqum-Oman," *Renewable and Sustainable Energy Reviews*, vol. 14, no. 2. Pergamon, pp. 821–827, 01-Feb-2010.

[30] S. Alexopoulos and B. Hoffschmidt, "Solar tower power plant in Germany and future perspectives of the development of the technology in Greece and Cyprus," *Renew. Energy*, vol. 35, no. 7, pp. 1352–1356, Jul. 2010.

[31] P. Palenzuela, G. Zaragoza, and D. C. Alarcón-Padilla, "Characterisation of the coupling of multi-effect distillation plants toconcentrating solar power plants," *Energy*, vol. 82, pp. 986–995, Mar. 2015.

[32] M. E. Demir and I. Dincer, "Development of an integrated hybrid solar thermal power system with thermoelectric generator for desalination and power production," *Desalination*, vol. 404, pp. 59–71, Feb. 2017.

[33] J. I. Ortega, J. I. Burgaleta, and F. M. Téllez, "Central Receiver System Solar Power Plant Using Molten Salt as Heat Transfer Fluid," *J. Sol. Energy Eng.*, vol. 130, no. 2, p. 024501, May 2008.

[34] P. Falcone, "A handbook for solar central receiver design," 1986.

[35] Z. Yao, Z. Wang, Z. Lu, and X. Wei, "Modeling and simulation of the pioneer 1 MW solar thermal central receiver system in China," *Renew. Energy*, vol. 34, no. 11, pp. 2437–2446, Nov. 2009.

[36] S. Benammar, A. Khellaf, and K. Mohammedi, "Contribution to the modeling and simulation of solar power tower plants using energy analysis," *Energy Convers. Manag.*, vol. 78, pp. 923–930, 2014.

[37] "seatemperature." [Online]. Available: www.seatemperature.info. [Accessed: 20-Aug-2018].

[38] "ASHRAE Climate Data Center." [Online]. Available: https://www.ashrae.org/technical-resources/bookstore/ashrae-climate-data-center. [Accessed: 28-Mar-2019].

[39] IRIMO, "I.R.OF IRAN Meteorological Organization archives." [Online]. Available: http://irimo.ir/eng/index.php. [Accessed: 18-Jan-2019].

[40] "worldweatheronline." [Online]. Available: https://www.worldweatheronline.com/. [Accessed: 20-Aug-2018].

[41] "Meteonorm." [Online]. Available: www.Meteonorm.com. [Accessed: 20-Aug-2018].

[42] N. Fazeli, H. Rezai, and R. Zare, "Spatial and Temporal Distribution of Oncaeidae in Chabahar Bay , Gulf of Oman," *researchgate.net*, vol. 6, pp. 216–220, 2012.

[43] A. A. Bidokhti and M. Ezam, "The structure of the Persian Gulf outflow subjected to density variations," *Ocean Sci.*, vol. 5, no. 1, pp. 1–12, 2009.

[44] F. Rahimzadeh, M. Pedram, and M. C. Kruk, "An examination of the trends in sunshine hours over Iran," *Meteorol. Appl.*, vol. 21, no. 2, pp. 309–315, Apr. 2014.

[45] X. Li, W. Kong, Z. Wang, C. Chang, and F. Bai, "Thermal model and thermodynamic performance of molten salt cavity receiver," *Renew. Energy*, vol. 35, no. 5, pp. 981–988, 2010.

[46] K. WARK, JR., *Advanced Thermodynamics For Engineers . New York: McGraw -Hill.* 1995.

[47] P. Palenzuela, D.-C. Alarcón-Padilla, and G. Zaragoza, *Concentrating Solar Power and Desalination Plants*. 2015.

[48] A. Lazzaretto and G. Tsatsaronis, "SPECO: A systematic and general methodology for calculating efficiencies and costs in thermal systems," *Energy*, vol. 31, no. 8–9, pp.

1257–1289, 2006.
[49] N. Kahraman and Y. A. Cengel, “Exergy analysis of a MSF distillation plant,” *Energy Convers. Manag.*, vol. 46, no. 15–16, pp. 2625–2636, 2005.
[50] R. Petela, “Exergy of Heat Radiation,” *J. Heat Transfer*, vol. 86, no. 2, p. 187, 1964.
[51] J. I. Burgaleta, S. Arias, and D. Ramirez, “Gemasolar: The First Tower Thermosolar Commercial Plant with Molten Salt Storage System,” in *SolarPACES*, 2013.
[52] P. Gilman and A. Dobos, “System Advisor Model, SAM 2011.12.2: General Description,” 2012.
[53] B. Rahimi and H. T. Chua, *Low grade heat driven multi-effect distillation and desalination*. 2017.
[54] M. H. Sharqawy, J. H. Lienhard V, and S. M. Zubair, “Erratum to Thermophysical properties of seawater: A review of existing correlations and data,” *Desalin. Water Treat.*, vol. 29, no. 1–3, pp. 355–355, Apr. 2011.
[55] H. T. El-Dessouky and H. M. Ettouney, *Fundamentals of salt water desalination*. Elsevier, 2002.